catalysts

MDPI

Article

Photocatalytic Degradation of Methylene Blue under Visible Light Using TiO_2 Thin Films Impregnated with Porphyrin and Anderson-Type Polyoxometalates (Cu and Zn)

Alexander Sanguino [1], Carlos Diaz-Uribe [1], Freider Duran [1], William Vallejo [1,*], Leidy Guzman [1], Daniela Ruiz [1], Esneyder Puello [2], Cesar Quiñones [3], Eduardo Schott [4,5] and Ximena Zarate [6]

1 Grupo de Fotoquímica y Fotobiología, Facultad de Ciencias Básicas, Universidad del Atlántico, Puerto Colombia 81007, Colombia
2 Grupo de Investigación en Oxi/Hidrotratamiento Catalítico y Nuevos Materiales, Facultad de Ciencias Básicas, Universidad del Atlántico, Puerto Colombia 81007, Colombia
3 Departamento de Física, Facultad de Ciencias, Universidad Nacional de Colombia, Bogotá 111321, Colombia
4 Departamento de Química Inorgánica, Facultad de Química y Farmacia, Centro de Energía UC, Centro de Investigación en Nanotecnología y Materiales Avanzados CIEN-UC, Pontificia Universidad Católica de Chile, Avenida Vicuña Mackenna, Santiago 4860, Chile
5 Millenium Nuclei on Catalytic Processes towards Sustainable Chemistry (CSC), Concepción 4030000, Chile
6 Instituto de Ciencias Químicas Aplicadas, Facultad de Ingeniería, Universidad Autónoma de Chile, Avenida Pedro de Valdivia 425, Santiago 7500912, Chile
* Correspondence: williamvallejo@mail.uniatlantico.edu.co; Tel.: +57-5359-9484

check for updates

Citation: Sanguino, A.; Diaz-Uribe, C.; Duran, F.; Vallejo, W.; Guzman, L.; Ruiz, D.; Puello, E.; Quiñones, C.; Schott, E.; Zarate, X. Photocatalytic Degradation of Methylene Blue under Visible Light Using TiO_2 Thin Films Impregnated with Porphyrin and Anderson-Type Polyoxometalates (Cu and Zn). *Catalysts* **2022**, *12*, 1169. https://doi.org/10.3390/catal12101169

Academic Editor: Roberto Fiorenza

Received: 9 September 2022
Accepted: 29 September 2022
Published: 4 October 2022

Abstract: In this work, tetra(4-carboxyphenyl)porphyrin (TCPP) and two Anderson-type polyoxomolybdates (containing Cu and Zn, respectively; CuPOM, ZnPOM) were synthesized and deposited on TiO_2 thin films. The properties of the obtained materials were characterized through UV–vis spectroscopy, Fourier transform infrared spectroscopy (FT-IR), diffuse reflection spectroscopy, scanning electron microscopy (SEM) and energy-dispersive X-ray spectroscopy (EDX). The adsorption and photodegradation under the visible light irradiation of methylene blue (MB) were studied for TiO_2, TCPP/TiO_2, TCPP/CuPOM/TiO_2 and TCPP/ZnPOM/TiO_2 thin films in aqueous solution. The results of the diffuse reflectance showed two bands in the visible light spectrum for the TCPP/POM/TiO_2 systems compared to unmodified TiO_2 that does not show any bands in the same region of the spectrum. The TCPP/POM/TiO_2 systems showed a higher removal of MB, with an adsorption rate near to 31% for the TCPP/CuPOM/TiO_2 film compared to 9% adsorption on the TiO_2 film. The kinetic results show that the pseudo-second order model was the best fitting model for the MB adsorption process onto fabricated materials. The photodegradation studies under visible light showed a better performance on TCPP/POM/TiO_2 thin films, with an efficiency in the MB photodegradation of near 49% and 44% in aqueous solution for TCPP/CuPOM/TiO_2 and TCPP/ZnPOM/TiO_2, respectively. The reusability test indicated that the porphyrin films are moderately stable after the performed cycles.

Keywords: heterogeneous photocatalysis; TiO_2; thin films; Anderson-type polyoxometalates; porphyrin

1. Introduction

The decontamination of bodies of water with several kinds of pollutants is a current challenge for water purification technologies. Therefore, there is a lot of effort in the study and implementation of advanced oxidation processes due to the flaws of conventional methods in the treatment of recalcitrant pollutants [1]. However, these methods have difficulties when applied on an industrial scale, such as high operating costs, the generation of toxic waste, the complexity of operating variables and the incapacity of using sunlight as a radiation source [2]. An example of an advanced oxidation process is heterogeneous photocatalysis. This process has been widely researched as an alternative for pollutant

degradation. It consists of the irradiation of a catalyst surface with enough energy to generate photoexcitation, producing highly oxidizing species that allow the degradation or mineralization of pollutants on a liquid or gaseous phase [3]. In photocatalysis, semiconductors (e.g., SnO_2, ZnO or TiO_2 [4]) and hybrid materials (quantum dots, composites [5–7]) are usually used as the active phase. The TiO_2 surface chemical properties rely on the electronic properties of the semiconductor surface, and it is one of the reasons for its high interest in photocatalytic applications [8]. However, TiO_2 has a low quantum efficiency in charge-carrier generation, which affects its photocatalytic activity [9], thus the use of superficial and structural modifications to increase the time for charge recombination of the carriers has been studied [10]. Different strategies have been implemented to improve the photocatalytic properties of TiO_2 (e.g., semiconductor coupling, doping and natural and synthetic sensitization) [11–14]. Among alternative compounds to modify the TiO_2 surface, the polyoxometalates (POMs) are a type of material that has gained a lot of interest due to its photocatalytic applications as well as its role in the modification of TiO_2 [15,16]. POMs are considered anionic molecular aggregates consisting primarily of transition metals in their highest oxidation state coordinated with oxygen atoms [17]. Anderson-type polyoxometalates are one of the classic structures of these materials. These POMs have six MO_6 octahedra (M = Mo^{VI} or W^{VI}) bonded around a central metallic atom (X) and a D_{3d} symmetry point group [18]. It has been found that the structural heteroatom on the POM has an important contribution to the HOMO-LUMO energy gap [19]. These orbitals can interact with the electronic bands of the TiO_2 having the capability to accept substrate photogenerated electrons, therefore reducing the charge recombination on TiO_2 and allowing a better absorptivity in the UV spectrum [20]. Both the POM and the TiO_2 have photocatalytic activity in the UV spectrum. The absorption at this wavelength is a disadvantage on an industrial scale due to the high operating cost and the limitation of using only a small amount of the photons that hit the earth surface. The hybrid systems, POM/TiO_2, have been reported as suitable catalysts in photocatalytic applications. Yu et al. synthesized the TiO_2/poly-oxo-tungstate composite and tested it in 2,4-dichlorophenol degradation. They reported that the composite led to the fastest 2,4-dichlorophenol degradation [21]. Jin et al. reported the efficient photocatalytic degradation of textile dye X-3B using polyoxometalate–TiO_2 hybrid materials [22]. Tang et al. modified the TiO_2 surface with Fe-containing polyoxometalates; they reported 33-times higher activity than a single photocatalyst in the bisphenol A degradation [23]. Su et al. reported an improvement in the oxidative desulfurization of fuel by TiO_2 quantum dot catalysts modified with Anderson-type polyoxometalate [24].

Furthermore, it has been observed that the sensitization of TiO_2 with synthetic (e.g., organometallic complex, porphyrin phthalocyanines [25,26]) and natural dyes (anthocyanins, chlorophyll, betalains [27–29]) is a typical strategy to improve both the TiO_2 photoactivity at the visible range of the electromagnetic spectrum and the photocatalytic performance. Among these sensitizers, porphyrins have conjugated cyclic and aromatic structures so they are easily reduced, can absorb visible light and coordinate with metals, making them attractive for photocatalytic applications [30,31]. Su et al. modified TiO_2 by using two copper porphyrins, and they reported that the composite exhibited higher photocatalytic activity than bare TiO_2 in the photodegradation of 4-nitrophenol [32]. Zhang reported the improvement in photocatalytic activity in porphyrin-sensitized TiO_2 nanorods in the degradation of 4-nitrophenol [33]. Otieno modified TiO_2 with meso-tetra(4-bromophenyl)porphyrins and their Zn(II), In(III), Ga(III) complexes and reported POM/TiO_2 composites with superior photocatalytic hydrogen generation compared to bare TiO_2 [34]. Zhu et al. reported (POMs)-porphyrin hybrids with photocatalytic application under visible irradiation [35], and Li et al. reported the fabrication of the ternary compound phthalocyanine/POM/TiO_2 photoanode for DSSC application [36].

In this report, the TiO_2 thin layers impregnated with Anderson-type polyoxometalates (CuPOM y ZnPOM) and porphyrin (tetra(4-carboxyphenyl)porphyrin) were employed for the photocatalytic degradation of methylene blue (MB) under visible light irradiation.

2. Results and Discussion

2.1. Materials Characterization

2.1.1. UV–Vis Characterization

The UV–vis spectra of the CuPOM y ZnPOM polyoxometalates (Figure 1) show a strong absorption peak near 280 nm. This band is characteristic of this type of material and corresponds to the charge transfer processes happening due to the material excitation, specifically of the ligand→metal type (LMCT); in this case, the O→Mo on a wavelength interval between 200 and 350 nm [37,38]. Furthermore, regarding the TCPP (Figure 1), there is evidence of the typical behavior of porphyrins. The spectra of the TCPP show a Soret band near 420 nm (transition $S_0 \rightarrow S_2$) and four Q bands (transition $S_0 \rightarrow S_1$) on the region between 500 nm and 660 nm of the visible spectrum [30,39]. These bands are generated by the conjugated cyclic and aromatic structures of the porphyrins.

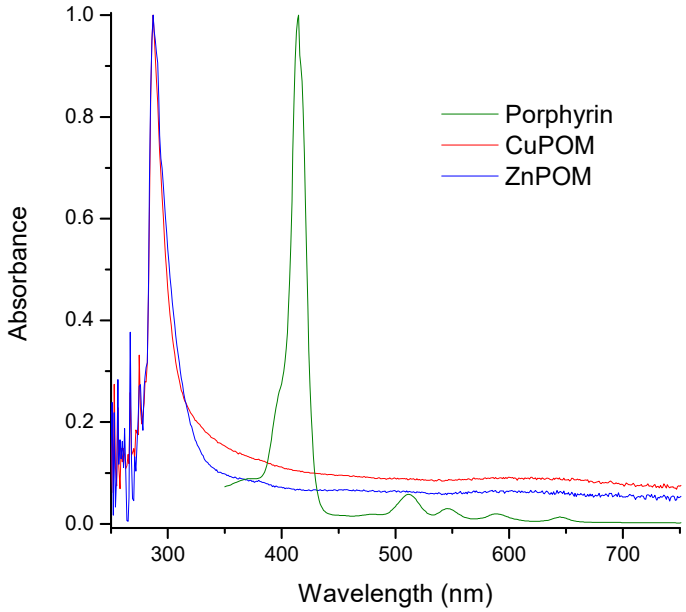

Figure 1. UV-vis spectra of TCPP, CuPOM and ZnPOM.

2.1.2. FT-IR Characterization

The FT-IR spectra of compounds synthesized in this work are shown on Figure 2. The FT-IR spectra of TCPP shows a peak near 1695 cm^{-1} associated with the vibrations of the C=O bond of the carboxylic acid group, which is characteristic of the porphyrin. The peaks near 1265 cm^{-1} and 1225 cm^{-1} correspond to the stretching modes of the C-O bond. The signals associated with the vibrations of the C=C and C=N bond appear on the peaks at 1605 cm^{-1} and 1565 cm^{-1}, respectively [40]. The FTIR spectra of CuPOM show signals located near 883 cm^{-1} and 801 cm^{-1}; these peaks are associated with the stretching vibrations of the Mo=O bond from the polyoxometalate [41]. There are also two weak signals around 567 cm^{-1} and 460 cm^{-1}, corresponding to the vibrations of the Cu-O-Mo bond; the strong signal at 630 cm^{-1} corresponds to the Mo-O-Mo bond vibrations [42,43]. On the other hand, the signals associated with the -OH stretching group are identified at 3500 and 3200 cm^{-1}.

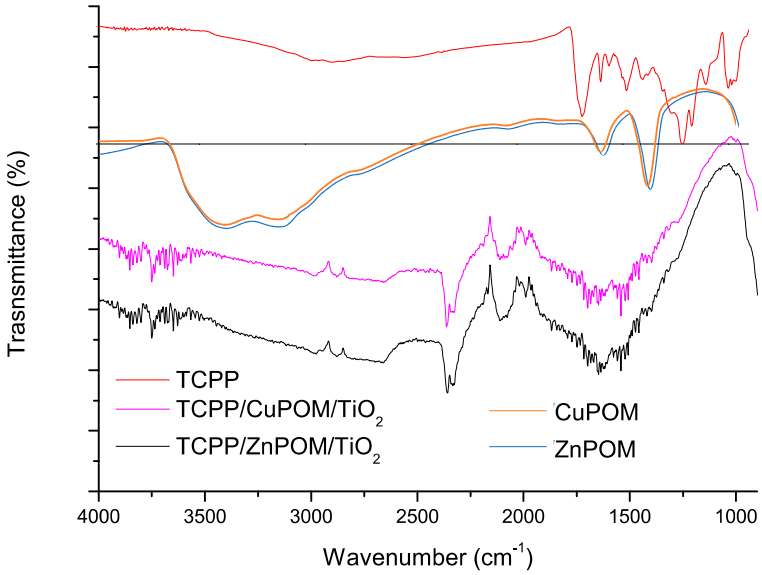

Figure 2. FT-IR spectra of TCPP, CuPOM, ZnPOM, TCPP/CuPOM/TiO_2 and TCPP/ZnPOM/TiO_2.

The ZnPOM FTIR spectra and interpretation are similar to the one of CuPOM. The similitude is because both are very similar Anderson-type POMs, and according to the literature, they have characteristic peaks near each other [44]. Regarding the FT-IR spectra of TCPP/CuPOM/TiO_2 and TCPP/ZnPOMTiO_2 (Figure 2), these systems show similar spectra to each other because the materials only differ on the heteroatom of the POM. The groups of signals located between 3800 cm^{-1} and 3600 cm^{-1} could be attributed to symmetric and antisymmetric vibrations of the O-H group from the water molecules and the stretching of the –NH group [45]. In the spectra of these systems, it is possible to identify the peaks associated with the stretching and angular deformation of the –NH group from the NH_4^+ counterion, corresponding to the peaks near 1400 and 3000 cm^{-1}. There is a peak near 1600 cm^{-1} associated with movements of the -OH group at 3400 and 1600 cm^{-1} [46]. On the other hand, on both systems, there are two signals near 1630 and 1381 cm^{-1} associated with the symmetric and antisymmetric vibrational modes of the $–CO_2^-$ group. According to the literature, when the TCPP is adsorbed on the TiO_2 surface, the bands from the C-O and C=O groups decrease their intensity, producing the appearance of the $–CO_2^-$ group signal. This could be explained due to the chemisorption of the TCPP carboxylic acid group as carboxylate on the TiO_2 surface.

2.1.3. Morphological Characterization

Figure 3 shows the SEM images of the TiO_2 films and the TCPP/POM/TiO_2 systems. Holes on the TiO_2 film could be observed, which could be due to the formation of bubbles during the elaboration of the thin film. Both the TCPP/CuPOM/TiO_2 and TCPP/ZnPOM/TiO_2 have a partially uniform surface with rugosity and pores. Furthermore, there are agglomerations of around 5 µm, only observed in the case of the modified surface. Table 1 summarizes the percentage composition of elements found with the EDS analysis. On the porphyrin/POM/TiO_2 films, it was possible to detect Mo and the heteroatoms of the studied Anderson structures. This result and the signals observed on the IR spectra confirm the presence of the CuPOM and ZnPOM impregnated on the TiO_2 films. Furthermore, both C and N were detected, confirming the porphyrin deposition on the photocatalyst.

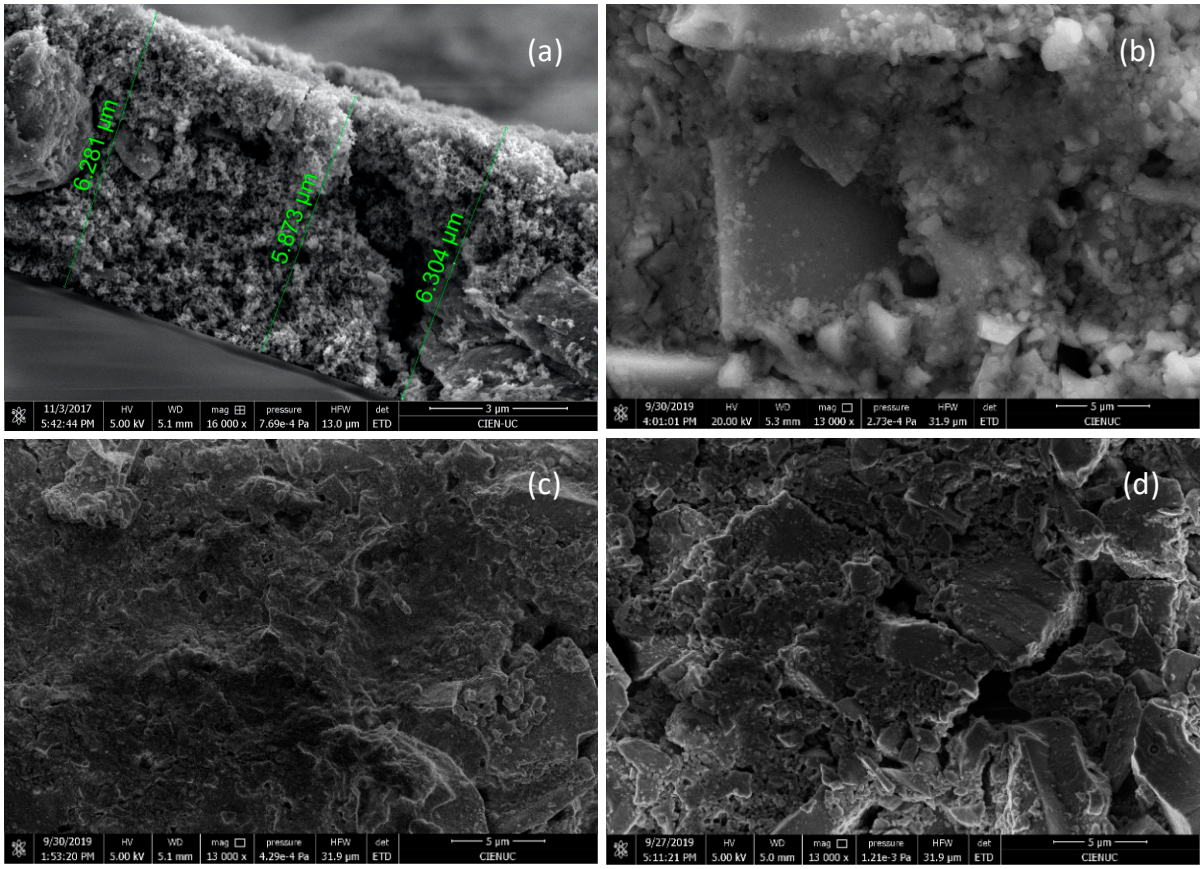

Figure 3. (**a**) Cross-section SEM ×18,000 image of the TiO_2 films. SEM ×13,000 images of the films: (**b**) TiO_2, (**c**) TCPP/CuPOM/TiO_2 and (**d**) TCPP/ZnPOM/TiO_2.

Table 1. Elemental composition analysis where Mo/X is the atomic relation between molybdenum and the Cu or Zn heteroatom.

Film *	% Ti	% O	% Mo	% X **	% C	% N
TiO_2	33.32	66.68	-	-	-	-
TCPP/CuPOM/TiO_2	15.34	66.85	0.39	0.07	15.78	1.60
TCPP/ZnPOM/TiO_2	20.81	66.72	0.48	0.18	10.71	1.11

* The film composition was obtained using EDS characterization results. ** X = Cu or Zn.

Taking into consideration the Mo and heteroatom percentages, the atomic relation Mo/X was calculated on the TCPP/POM/TiO_2 films, which theoretically should be around 6 for Anderson-type POMs [47].

It was found that this relation is only experimentally met for the TCPP/CuPOM/TiO_2. This finding could be explained as the EDS technique is a microanalysis performed over a punctual sector of the sample, and the results are influenced by the size of particles found at the site where the procedure is performed [48]. The same explanation could be given to the decrease in the Ti signal for the TCPP/POM/TiO_2 sample in comparison to the bare TiO_2. Another relevant aspect regarding the composition results (Table 1) is the increment on the signal generated by O atoms on the TCPP/ZnPOM/TiO_2 and TCPP/CuPOM/TiO_2 films in comparison to the signal found for the bare TiO_2. This is attributed to the contribution of the Anderson POMs supported on the TiO_2.

2.1.4. Optical Characterization

Figure 4 shows the reflectance spectra for TiO_2, TCPP/ZnPOM/TiO_2 and TCPP/CuPOM/TiO_2. There is a shift on the absorption spectra of the modified materials compared with the unmodified TiO_2 thin films, obtaining two pronounced absorption bands around 420 nm and

550 nm. The differences on the absorption peaks of both materials could be due to the different molar absorption coefficients of copper and zinc polyoxometalates.

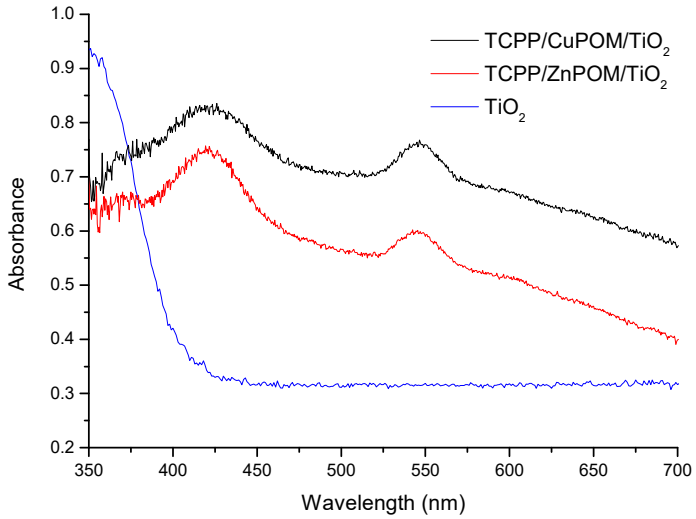

Figure 4. Reflectance diffuse spectra of the studied materials.

Taking into consideration the UV–vis results for the POMs and porphyrins where there is evidence that TCPP absorbs visible light, while CuPOM and ZnPOM absorb only on the UV region (see Figure 1), the absorption of visible light for the modified systems could be attributed mainly to TCPP. This effect of the porphyrins has been widely reported in TiO_2 sensitization studies, such as absorption studies on the visible region by porphyrins with and without transition metals, supported on TiO_2, to decompose MB [31]. It has been found that TCPP sensitized on TiO_2 has a UV-vis spectra similar to TCPP alone. The main difference is the fact that the carboxylate group improves the electronic coupling on the porphyrin π^* orbitals and the Ti *3d* orbital, stabilizing the π^* orbital by delocalization [49]. According to the literature, the interaction mechanism of the porphyrin with the TiO_2 is based on the band gap energy of these two materials. The energy difference between the valence band (VB) and the conduction band (CB) of bare TiO_2 is around 3.2 eV. Thus, for an electronic transition to occur, the TiO_2 needs to absorb only ultraviolet light, which is less abundant than visible light. All the porphyrins have a strong absorption from 400 to 450 nm (Q band) and absorption peaks from 500 to 700 nm, so its electronic excitation can occur on the visible light spectrum. Figure 4 shows there is no absorption above 400 nm for the unmodified TiO_2 thin films, while the TCPP/POM/TiO_2 thin films show typical porphyrin absorption signals. This result suggests that porphyrin was anchored to the TiO_2 surface [31,50].

2.2. Adsorption and Kinetic Study

All the isotherms in Figure 5 have an L shape according to the adsorption isotherm classification, meaning there is no strong competition between water and the pollutant molecules to occupy the sites on the TiO_2 surface [51]. Table 2 summarizes the calculated parameters from the Freundlich and Langmuir models using minimal squares linear regression. Based on the linear regression coefficients, the experimental isotherm of the modified films better fit the Langmuir model, indicating a monolayer adsorption model. It has been reported that the adsorption isotherms of porphyrins supported on substrates, which capture cationic pollutants, adjust better with the Langmuir model [52]. The Langmuir constant K_L expresses adsorption affinity [53]; it was found that the TCPP/CuPOM/TiO_2 and TCPP/ZnPOM/TiO_2 films have the highest values of K_L in comparison to bare TiO_2 and TCPP/TiO_2., thus implying a higher affinity for MB of the TCPP/CuPOM/TiO_2 and TCPP/ZnPOM/TiO_2 films. The bare TiO_2 film better fits the Freundlich model, indicating

that the MB is adsorbed on multiple layers over the film surface [54]. This result for the bare TiO_2 is in concordance with other reports from the literature [55,56].

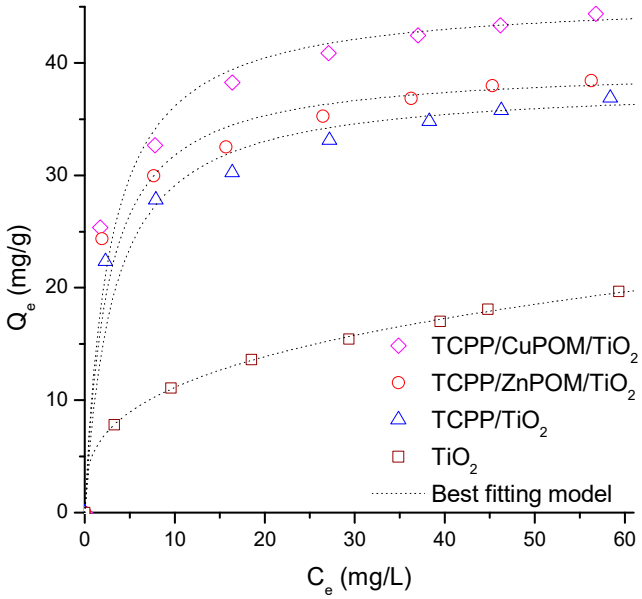

Figure 5. Experimental isotherm data for MB adsorption onto composite films. Inside the figure, the best fitting model is shown (Freundlich to TiO_2 and Langmuir isotherm to the rest of the materials).

Table 2. Fitting results of Langmuir and Freundlich isotherm models.

Model Fitting	Parameters *	TiO_2	TPCC/ TiO_2	TPCC/ CuPOM/TiO_2	TPCC/ ZnPOM/TiO_2
Freundlich	K_F $(mg/g)/(mg/L)^n$	5.420	19.869	23.507	22.452
	1/n	0.312	0.153	0.163	0.1365
	R^2	0.999	0.996	0.991	0.997
Langmuir	q_m (mg/g)	21.645	38.168	45.872	39.682
	K_L (L/mg)	0.109	0.321	0.372	0.402
	R^2	0.987	0.998	0.998	0.998

* Parameters obtained from the fitting data of Figure 5.

2.3. Kinetic Study

Figure 6 shows the methylene blue adsorption kinetics onto the thin films, and Table 3 lists the kinetic results. For this, measurements were performed every 5 min until reaching equilibrium, with an MB starting concentration of 10 mg/L. The percentage of adsorbed pollutant was 30.8% and 28.1% for the TCPP/CuPOM/TiO_2 and TCPP/ZnPOM/TiO_2 systems, respectively, which was superior to the results for the TCPP/TiO_2 and bare TiO_2 films (26.1% and 9%, respectively). The ternary systems also reached the adsorption–desorption equilibrium more rapidly than the TCPP/TiO_2 and bare TiO_2 films, with values of 35 min for the TCPP/POM/TiO_2 thin films.

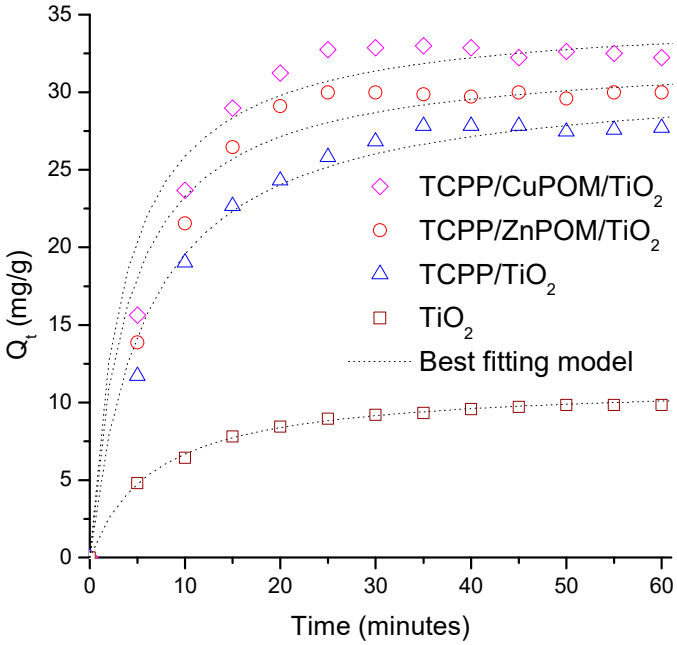

Figure 6. Experimental kinetic data for MB adsorption onto thin films. Inside the figure, the best fitting model is shown (pseudo-second model).

Table 3. Results at equilibrium concentration.

Parameters *	TiO_2	TPCC/ TiO_2	TPCC/ $CuPOM/TiO_2$	TPCC/ $ZnPOM/TiO_2$
Time for equilibrium	50	35	30	25
MB adsorbed (%)	9.0	26.1	30.8	28.1
Concentration at equilibrium (mg/g)	9.8	27.8	32.9	30.0

* Parameters obtained from the data of Figure 6.

The films with the TCPP adsorbed a higher percentage of pollutant than the bare TiO_2. This could be due to the electrostatic interactions between the nitrogen atoms of the porphyrin and the MB (of cationic nature). Hou et al. reported that the electrostatic interactions between the noncoordinated nitrogen atoms of the porphyrin with the MB play an important role in the increase in the adsorption percentage on the surface of the semiconductor material [57]. The results also show a significant difference in MB adsorption for the $TCPP/CuPOM/TiO_2$ and $TCPP/ZnPOM/TiO_2$ relative to bare TiO_2. The Anderson-type POMs are of an anionic nature, so there is a higher attraction between the POMs and MB, resulting in a better adsorption on the films [58]. Thus, a better adsorption for the ternary systems due to the anionic nature of POMs is observed in this report, attributed to the electrostatic interactions of noncoordinated nitrogen from the TCPP molecules and the oxygen atoms of the titanium oxide (synergistic effect).

To study the adsorption kinetics on the films and evaluate the correlation degree or fit of the experimental data, pseudo-first order and pseudo-second order mathematical models were used (see Table 4). These mathematical models have been widely used to identify the dynamic of adsorption processes [59]. According to previous research on the adsorption processes of methylene blue on modified and nonmodified TiO_2 films, it is possible that more than one model fits the experimental data because a coefficient near to 1 could be obtained in the correlation. This would mean that several types of adsorption processes participate in the adsorption of the studied pollutant [60,61].

Table 4. Adsorption kinetic parameters using pseudo-first order, pseudo-second order and Elovich coefficient models.

Kinetic Model Fitting	Parameters	TiO_2	TPCC/ TiO_2	TPCC/ ZnPOM/TiO_2	TPCC/ CuPOM/TiO_2
Pseudo-first *	k_1 (min^{-1})	0.0893	0.1074	0.1715	0.2043
	q_e Calculated	8.60	27.37	36.75	51.60
	R^2	0.969	0.976	0.968	0.911
Pseudo-second *	k_2 ($min^{-1}.M^{-1}$)	0.014	0.0054	0.0078	0.0080
	q_e Calculated	11.0	31.15	32.5	35.1
	R^2	0.999	0.995	0.994	0.994

* Parameters obtained from the fitting data of Figure 6.

The pseudo-second order model showed the best fitting regression values (higher R^2, Table 4). These results suggest that chemisorption is the dominant interaction during the adsorption of methylene blue onto the catalyst, where effective electrostatic interactions play an important role in adsorption, and a chemical reaction (e.g., complexation) could be present during the adsorption process. Furthermore, the chemisorption process involved attracting forces generated by valence or electron exchange between the adsorbent and adsorbate [53]. In the particular case of the TCPP/ZnPOM/TiO_2 film, a R^2 of 0.9678 was obtained for the pseudo-first order model, indicating that, besides the chemisorption, there is also a physisorption involved due to the electrostatic attraction of the involved species. Finally, our results agree with other studies where the nonmodified TiO_2 film fitted the pseudo-second order model [62].

2.4. Photocatalytic Study

Figure 7a shows the methylene blue concentration as a function of time under visible irradiation, and Figure 7b shows the pseudo-first order Langmuir–Hinshelwood (LH) model fitting [60]. According to the literature, the Langmuir–Hinshelwood (L-H) kinetic model is widely used to analyze the degradation kinetic of pollutants in aqueous phase [63].

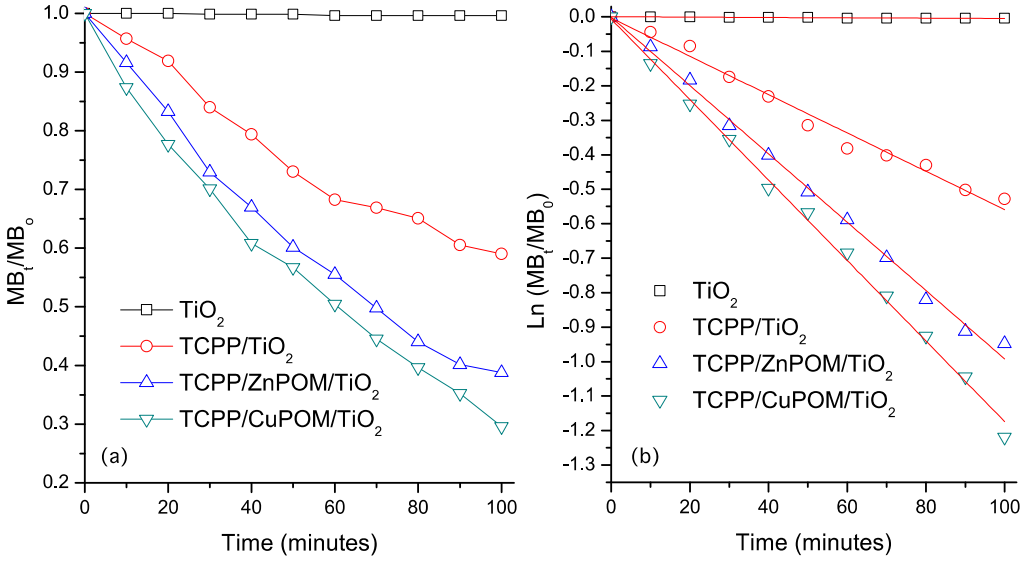

Figure 7. (**a**) Methylene blue (MB) concentration vs. time of visible irradiation. (**b**) Experimental data fitting with the Langmuir–Hinshelwood model.

Figure 7a shows the removal percentage of MB through photodegradation in the visible light spectrum. The results show an improvement in the photocatalytic activity on

the systems by means of the addition of the porphyrins and POMs compared to the bare TiO_2 film. The observed trend for the obtained results is (from best to worst photocatalyst): TCPP/CuPOM/TiO_2 > TCPP/ZnPOM/TiO_2 > TCPP/TiO_2 > TiO_2. As explained before, this result is associated with the effect of the porphyrin on the photocatalytic improvement of TiO_2 due to electronic migration processes [33,34]. Thus, when the TCPP is attached to the TiO_2, the excited electrons can migrate to the conduction band of the TiO_2. These reactive electrons in the conduction band reduce the adsorbed O_2 on the TiO_2 surface to $^{\bullet}O_2^-$, which can degrade pollutants such as MB. Furthermore, the holes on the TiO_2 can turn H_2O into $^{\bullet}OH$, which also can degrade pollutants such as MB to CO_2 and H_2O [31,64].

The TCPP/POM/TiO_2 system has better performance than the TiO_2 and TCPP/TiO_2 films. This proves that the porphyrin and the POM significantly contribute to the improvement of the photocatalytic activity of TiO_2 in the visible light spectrum. This could be related to the ability of the porphyrin to absorb visible light, unlike TiO_2 and the POM. Furthermore, by being able to migrate electrons to the TiO_2 conduction band, it allows the model pollutant to be degraded. However, due to its POM redox properties, it is also possible for the porphyrin to transfer electrons directly to the POM. This could make the POM a reactive species contributing to the degradation of the model pollutant. There are previous studies that report the combined or cooperative effect of porphyrins and transition metals or porphyrins with POMs to decompose pollutants [65,66]. Therefore, there would be a synergistic effect between the porphyrin and POM for the TCPP/CuPOM/TiO_2 and TCPP/ZnPOM/TiO_2 systems.

Figure 7b shows the experimental data fitting using the Langmuir–Hinshelwood model, and Table 3 summarizes the kinetic parameters. The behavior of TiO_2 in Figure 7b is a straight line with a slope close to zero as the TiO_2 does not degrade the model pollutant and has no photocatalytic activity under visible light irradiation [63]. Table 5 shows a comparison of the reaction rate constants of the modified materials compared to the bare TiO_2 films. It was found that the modified materials have reaction rates over 100 times greater than the bare TiO_2 irradiated in the visible range. From the materials studied, the TCPP/POM/TiO_2 systems are the fastest, especially the copper thin layer. There is also a comparison between the reaction rates of the TCPP/POM/TiO_2 systems and the TCPP/TiO_2 film. The ternary systems degrade double the amount of MB than TCPP/TiO_2. This indicates that the addition of the POM improves the photocatalytic activity in systems with porphyrin. As mentioned before, a possible synergy due to the charge transfer processes from the porphyrin to the TiO_2 and POM would explain this behavior.

Table 5. Fitting results of Langmuir–Hinshelwood for the photocatalytic degradation of MB under visible irradiation *.

Thin Film	k_1 (min^{-1}) × 10^{-5}	R^2	$k_1/k_{1\text{-}TiO_2}$	$k_1/k_{1\text{-}TPCC}$
TiO_2	5.0	0.8646	-	-
TPCC/TiO_2	556	0.9834	112	-
TPCC/ZnPOM/TiO_2	991	0.9963	198	1.78
TPCC/CuPOM/TiO_2	1168	0.9970	234	2.10

* Parameters obtained from the fitting data of Figure 7.

The metal presence is important for the visible light absorption observed for these POMs, as it has been shown that POMs without any transition metal in their structure present a white color which would represent no photocatalytic activity in the visible region of the spectrum. Both the photocatalytic efficiency of the system as well as the kinetic parameters of the degradation curves prove that the TCPP/CuPOM/TiO_2 has the best photocatalytic activity on the visible spectrum. These results might be due to several factors. On the one hand, the presence of an unpaired electron in the case of the CuPOM, which has a Cu^{2+} as a transition metal. On the other hand, the difference observed, in the case of the ZnPOM, could be attributed to the presence of the Zn atom, which has 230, is not

a transition metal character and presents a saturated d atomic orbital (d^{10}); in addition, Zn(II) has shown a nonreducible character that would more easily give peroxo entities (ZnO2). In addition, based on the computational studies reported in the literature, this could be explained, as the copper POM is slightly more stable than the zinc POM, as their bonding energy decomposition is slightly higher, −154.8 eV for CuPOM and −153.4 eV for ZnPOM [45].

The stability of the catalysts is other important parameter in addition to the photocatalytic capacity. Figure 8a,b shows the results of the adsorption–photodegradation of MB under the visible light spectrum for TCPP/TiO_2, TCPP/CuPOM/TiO_2 and TCPP/ZnPOM/TiO_2 films. In Figure 8, the TiO_2 photocatalytic efficiency is not included as it is ~0.0 (see Figure 7a). After four consecutive cycles, the TiO_2 film does not significantly change its adsorption capacity. For adsorption, the total decrease was 0.3%, suggesting that the material was stable to constant in the adsorption/desorption process. These results are consistent with other studies performed with this material where, after four cycles, the adsorption capacity of MB is not significantly affected [53].

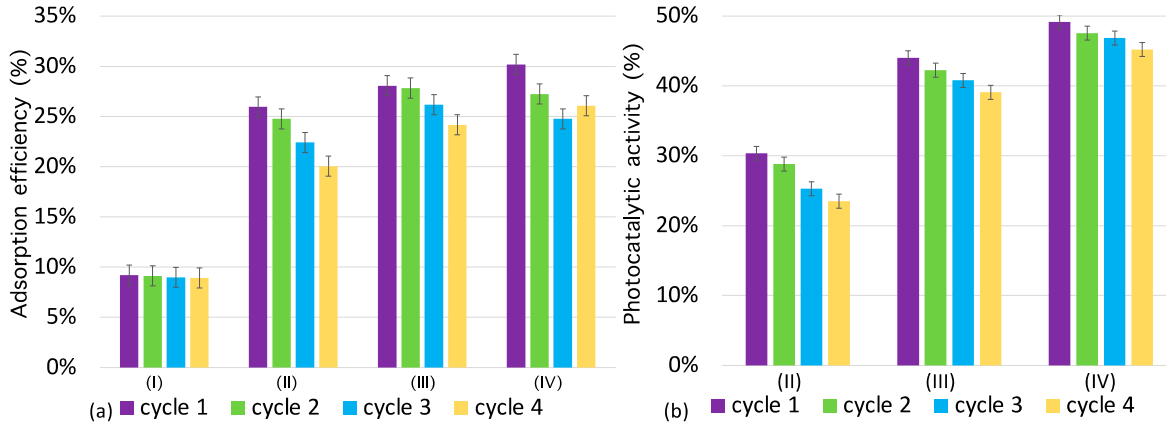

Figure 8. (**a**) Comparation among adsorption and (**b**) photocatalytic efficiency of modified and unmodified TiO_2 films after 4 cycles. Inside figure: (I) TiO_2, (II) TCPP/TiO_2, (III) TCPP/ZnPOM/TiO_2 and (IV) TCPP/CuPOM/TiO_2.

In the case of the TCPP/TiO_2 film, there was a decrease in adsorption and photocatalytic efficiency, with differences on the first and fourth cycles of 3.9% and 5.0%, respectively. The photodegradation results indicate that the material is moderately stable to visible radiation. On the other hand, for the TCPP/CuPOM/TiO_2 and TCPP/ZnPOM/TiO_2 films, there was a slighter decrease on their adsorption capacity and photodegradation compared with TCPP/TiO_2, where the total difference between the different cycles was around 4% and 4.5%, respectively. The better performance of these two materials in comparison to the photodegradation of TCPP/TiO_2 would obey the interactions between the Zn and Cu heteroatoms of the POM and the TiO_2, generating charge densities with a higher life span and a better degradation efficiency after a large number of cycles [31].

In general, the results obtained regarding the photodegradation capacity of the materials with porphyrin are consistent with previous studies where several type of porphyrins are supported on modified TiO_2, with differences after four cycles of about 10% [67,68].

3. Materials and Methods

3.1. Reagents

Polyoxometalates were synthesized using ammonium molybdate hexahydrate $(NH_4)_6[Mo_7O_{24}]\bullet 6H_2O$, copper nitrate trihydrate ($[Cu(NO_3)_2]\bullet 3H_2O$) or/and zinc nitrate hexahydrate ($[Zn(NO_3)_2]\bullet 6H_2O$). The tetra(4-carboxyphenyl)porphyrin (TCPP) synthesis was performed using: pyrrole, 4-carboxybenzaldehyde, propionic acid, nitrobenzene, sodium hydroxide, hydrochloric acid and ethanol. TiO_2 films were synthe-

sized using glass films as substrate and TiO_2—Degussa powder (P25), distilled water, isopropanol, titron ×100 and acetic acid as reagents. Finally, the photocatalytic test was performed using MB as a model pollutant.

3.2. Polyoxometalate Synthesis

The polyoxometalates were synthesized through coprecipitation in aqueous solution from the precursor salt containing the heteroatom (X = Cu, Zn) and ammonium molybdate hexahydrate, under constant stirring from the reagents mixture until the formation of the precipitate. To 30 mL of distilled water at 60 °C, the following was added: 3.37 mmol of $(NH_4)_6Mo_7O_{24}•4H_2O$ and 0.562 mmol of $[Cu(NO_3)_2]$; $•6H_2O$ to $(NH_4)_4[CuMo_6O_{24}H_6]•5H_2O$ (CuPOM); and 0.562 mmol of zinc nitrate hexahydrate ($[Zn(NO_3)_2]•6H_2O$) to $(NH_4)_4[CuMo_6O_{24}H_6]•5H_2O$ (ZnPOM) in a Mo/X = 6 stoichiometric proportion. The mixture was cooled at room temperature (28 °C). Afterwards, a solution 0.1 M NH_4Cl was added to the mixture in order to maintain the pH between 5 and 6. The mixture was left to stand for 12 h to ensure the precipitation of the product [69]. The solid obtained was filtered under vacuum and washed multiple times with distilled water to remove impurities. The solid was dried for 6 h at 105 °C in a natural convection oven. The reaction yield was 85% and 88% for CuPOM and ZnPOM, respectively.

3.3. Synthesis of Porphyrin

In order to obtain tetra(4-carboxyphenyl)porphyrin (TCPP), pyrrole was added to a mixture of 4-carboxybenzaldehyde (30 mmol), nitrobenzene (45 mL) and propionic acid (105 mL). The mixture was heated for 1 h at 120 °C. Then, the solvent was removed under vacuum, and the porphyrin was dissolved in 250 mL of NaOH (0.1 M). Finally, the porphyrin was precipitated with HCl (1M), redissolved using ethanol and recrystallized using solvent evaporation [70].

3.4. Fabrication of TiO_2 Thin Films

TiO_2–Degussa powder was deposited on glass using the doctor blade method. The substrate was cleaned in an ultrasonic cleaner tank filled with cleaning solution (neutral soap) for 20 min, then in distilled water for 20 min and finally in a distilled water/isopropanol 1:1 solution for 20 min. Afterwards, the films were dried at 105 °C in a natural convection oven for 1 h and left to stand at room temperature. A catalytic suspension was prepared mixing 2 g of TiO_2–Degussa P25, 0.5 g of polyethylene glycol 6000, 2 mL of water, 1 mL of acetic acid and 1 mL of triton ×100 (surfactant). The suspension was spread using a roller extended horizontally on soda lime glass as substrate (2.0 cm × 3.5 cm). The films were dried for 6 h at 90 °C and calcined for 2 h at 450 °C in a muffle. The thickness of the TiO_2 thin films was between 5.9 and 6.3 μm (see Figure 3a) [71,72].

3.5. Modification of Thin Films

The TCPP/TiO_2 films were deposited through impregnation by contacting the TiO_2 films with a TCPP solution in dimethylformamide (DMF). First, a 10 mg/L porphyrin solution in DMF was prepared. Then, the TiO_2 films were immersed in that solution under constant stirring for 12 h. After that, the films were dried and cooled to room temperature. The TCPP/CuPOM/TiO_2 and TCPP/ZnPOM/TiO_2 films were deposited through wet impregnation by contacting the TCPP/TiO_2 films with the prepared polyoxometalates aqueous solutions. In order to do this, 10 mg/L POM aqueous solutions was prepared and then the films were immersed in this solution under constant stirring for 12 h. Finally, the films were dried at 105 °C and then cooled to room temperature.

3.6. Characterization of Thin Films

The obtained films were characterized by UV–vis spectroscopy, Fourier transform infrared spectroscopy (FT-IR), scanning electron microscopy (SEM), energy-dispersive

X-ray spectroscopy (EDX) and diffuse reflectance spectroscopy (DRS). The UV–vis spectra were measured with a Thermo Scientific Evolution 220 V. The IR was measured with an ECO-ATR Alpha Bruker FTIR spectrophotometer. The samples were analyzed with a SEM equipment (QUANTA FEG 650 model) at 25.0 kV. For the chemical analysis, an EDAX APOLO X detector with a 126.1 eV resolution and EDX Genesis software for the semiquantitative information of the chemical elements were used. The diffuse reflectance measurements were performed with a Lambda 4 Perkin Elmer spectrometer equipped with an integration sphere. The thickness of the thin films was determined through cross-section SEM assay.

3.7. Methylene Blue Adsorption Studies

For the experimental study of adsorption kinetics, the reactor was filled with 100 mL of a 10 mg/L MB solution, and then a TiO_2 film was immersed in this reactor. The system was kept in the dark, and an aliquot was taken every 5 min to be analyzed in the UV–vis spectrometer. The process was monitored until the adsorption/desorption equilibrium was reached. This same procedure was applied to evaluate the TCPP/TiO_2 and TCPP/POM/TiO_2 systems. Then, an adsorption isotherm study was carried out for every film; in order to do this, the adsorption kinetic procedure was repeated varying the MB solution concentration to 5, 20, 30, 40, 50 and 60 mg/L. Furthermore, the kinetic and adsorption isotherm models were used to analyze the data obtained. Finally, the recyclability test was carried out. Four repetitive adsorption–desorption cycles were performed to determine the stability of the thin films after the adsorption process.

3.8. Photocatalytic Study under Visible Light Irradiation

For the photodegradation, a 100 mL closed reactor was used. A TCPP/TiO_2 film was immersed in the reactor filled with 100 mL of 10 mg/L methylene blue (MB) solution. The film was left in the dark until the equilibrium of the dye adsorption–desorption was obtained as described in the previous section. To reach adsorption–desorption equilibrium on the catalyst surface before irradiation, the MB solution was kept in the dark for 60 min at 250 rpm. Afterwards, the reactor was inserted in a device with two tubular visible light lamps. The system was irradiated with visible light for 5 h, and every 20 min, a solution sample was taken to determine the MB residual concentration. After 5 h, the system was kept under visible light irradiation until total discoloration of the solution. The tested films were removed and dried at 90 °C. The obtained data were fitted with the Langmuir–Hinshelwood (L-H) kinetic model in order to study the MB kinetic degradation. In addition, a reusability test was performed. In order to do this, the experiment was repeated with a new adsorption–photodegradation cycle using the same film to see how stable the film was; four cycles were performed in total. This procedure was repeated for all the studied films.

4. Conclusions

In this work, the double synergic effect of Anderson-type (ZnPOM and CuPOM) and a porphyrin anchored to TiO_2 thin films was studied. The TiO_2 thin films were fabricated using the doctor blade technique. Anderson-type polyoxometalates were synthesized by coprecipitation, and TCPP was synthesized using the Adler method. We studied the photocatalytic and adsorption properties of the materials. FT-IR on the TCPP/POM/TiO_2 systems showed interactions between POM and TCPP with the substrate. These results and the elemental analysis of EDX confirms the impregnation of porphyrin and POMs on the TiO_2 films. Diffuse reflectance spectroscopy showed two absorption peaks on the visible spectrum around 420 nm and 550 nm for the TCPP/POM/TiO_2 systems, confirming absorption of visible light for these modified materials. TCPP/CuPOM/TiO_2, TCPP/ZnPOM/TiO_2, TCPP/TiO_2 and TiO_2 films had a methylene blue adsorption capacity of ∼31%, 28%, 26% and 9%, respectively. The higher adsorption capacity of the TCPP/POM/TiO_2 systems can be explained by the electrostatic interactions between the

porphyrin and the model pollutant and due to the electric charge that the POMs confer to the TiO_2 film surface. Based on the photodegradation capability of MB under visible light, the TCPP/POM/TiO_2 system has a higher activity in comparison to the TCPP/TiO_2 and TiO_2 films. The TCPP/CuPOM/TiO_2 had the highest photocatalytic activity, degrading ~49% of MB, followed by TCPP/ZnPOM/TiO_2 with 44.04%, TCPP/TiO_2 with 30.36%, and lastly, TiO_2 which did not degraded MB. The higher photocatalytic activity of the ternary copper system over zinc is attributed to the slightly higher stability of the copper POM, implying a higher photocatalytic activity. The higher photocatalytic activity of the TCPP/POM/TiO_2 system was mainly associated with the electronic transfer processes from the TCPP to the TiO_2 and POM. The reusability tests of the modified materials showed that they are moderately stable after four cycles, and the TCPP/POM/TiO_2 showed the highest stability. The ternary systems had a performance improvement associated with the interactions between the Zn and Cu heteroatoms of the POM and the TiO_2.

Author Contributions: Conceptualization, C.D.-U., W.V.; methodology, C.D.-U., A.S., F.D., D.R., E.P. and C.Q.; validation, W.V., C.D.-U., A.S., F.D. and D.R.; formal analysis, W.V., C.D.-U., A.S. and L.G.; investigation, C.D.-U., A.S. and F.D.; resources, W.V. and C.D.-U.; data curation, W.V., C.D.-U. and A.S.; writing—original draft preparation, C.D.-U., W.V., A.S., E.S. and X.Z.; writing—review and editing, C.D.-U., W.V., A.S., C.Q., E.S. and X.Z.; visualization, C.D.-U. and W.V.; supervision, C.D.-U. and W.V.; project administration, C.D.-U. and W.V.; funding acquisition, W.V. and C.D.-U. All authors have read and agreed to the published version of the manuscript.

Funding: This research was funded by Universidad del Atlántico.

Data Availability Statement: Data is contained within the article.

Acknowledgments: C.D.-U. and W.V. would like to thank the Universidad del Atlántico. This work was funded by ANID, the Millennium Science Initiative Program, NCN2021_090; ANID/FONDAP/15110019; FONDECYT 1201880 and the Anillos de Ciencia y Tecnología ACT210057.

Conflicts of Interest: The authors declare no conflict of interest.

References

1. Khan, S.; Sayed, M.; Sohail, M.; Shah, L.A.; Raja, M.A. Advanced Oxidation and Reduction Processes. In *Advances in Water Purification Techniques: Meeting the Needs of Developed and Developing Countries*; Elsevier: Amsterdam, The Netherlands, 2019; pp. 135–164.
2. Brienza, M.; Katsoyiannis, I.A. Sulfate Radical Technologies as Tertiary Treatment for the Removal of Emerging Contaminants from Wastewater. *Sustainability* **2017**, *9*, 1604. [CrossRef]
3. Gopinath, K.P.; Madhav, N.V.; Krishnan, A.; Malolan, R.; Rangarajan, G. Present applications of titanium dioxide for the photocatalytic removal of pollutants from water: A review. *J. Environ. Manag.* **2020**, *270*, 110906. [CrossRef] [PubMed]
4. Li, X.; Yu, J.; Jiang, C. Principle and surface science of photocatalysis. *Interface Sci. Technol.* **2020**, *31*, 1–38.
5. Bakry, A.M.; Alamier, W.M.; Salama, R.S.; Samy El-Shall, M.; Awad, F.S. Remediation of water containing phosphate using ceria nanoparticles decorated partially reduced graphene oxide (CeO2-PRGO) composite. *Surf. Interfaces* **2022**, *31*, 102006. [CrossRef]
6. Alshorifi, F.T.; Alswat, A.A.; Mannaa, M.A.; Alotaibi, M.T.; El-Bahy, S.M.; Salama, R.S. Facile and Green Synthesis of Silver Quantum Dots Immobilized onto a Polymeric CTS-PEO Blend for the Photocatalytic Degradation of p-Nitrophenol. *ACS Omega* **2021**, *6*, 30432–30441. [CrossRef]
7. Alshorifi, F.T.; Alswat, A.A.; Salama, R.S. Gold-selenide quantum dots supported onto cesium ferrite nanocomposites for the efficient degradation of rhodamine B. *Heliyon* **2022**, *8*, e09652. [CrossRef]
8. Rahimi, N.; Pax, R.A.; Gray, E.M.A. Review of functional titanium oxides. I: TiO_2 and its modifications. *Prog. Solid State Chem.* **2016**, *44*, 86–105. [CrossRef]
9. Guo, Q.; Zhou, C.; Ma, Z.; Yang, X. Fundamentals of TiO_2 Photocatalysis: Concepts, Mechanisms, and Challenges. *Adv. Mater.* **2019**, *31*, 1901997. [CrossRef]
10. Du, J.; Lai, X.; Yang, N.; Zhai, J.; Kisailus, D.; Su, F.; Wang, D.; Jiang, L. Hierarchically Ordered Macro Charge Recombination, and Their Enhanced Photocatalytic Activities. *ACS Nano* **2011**, *5*, 590–596. [CrossRef]
11. Humayun, M.; Raziq, F.; Khan, A.; Luo, W. Modification strategies of TiO $_2$ for potential applications in photocatalysis: A critical review. *Green Chem. Lett. Rev.* **2018**, *11*, 86–102. [CrossRef]
12. Mergenbayeva, S.; Kumarov, A.; Atabaev, T.S.; Hapeshi, E.; Vakros, J.; Mantzavinos, D.; Poulopoulos, S.G. Degradation of 4-Tert-Butylphenol in Water Using Mono-Doped (M1: Mo, W) and Co-Doped (M2-M1: Cu, Co, Zn) Titania Catalysts. *Nanomaterials* **2022**, *12*, 2326. [CrossRef]

13. Rawal, S.B.; Bera, S.; Lee, D.; Jang, D.-J.; Lee, W.I. Design of visible-light photocatalysts by coupling of narrow bandgap semiconductors and TiO_2: Effect of their relative energy band positions on the photocatalytic efficiency. *Catal. Sci. Technol.* **2013**, *3*, 1822. [CrossRef]
14. Jaafar, S.N.H.; Minggu, L.J.; Arifin, K.; Kassim, M.B.; Wan, W.R.D. Natural dyes as TIO2 sensitizers with membranes for photoelectrochemical water splitting: An overview. *Renew. Sustain. Energy Rev.* **2017**, *78*, 698–709. [CrossRef]
15. Lauinger, S.M.; Sumliner, J.M.; Yin, Q.; Xu, Z.; Liang, G.; Glass, E.N.; Lian, T.; Hill, C.L. High Stability of Immobilized Polyoxometalates on TiO_2 Nanoparticles and Nanoporous Films for Robust, Light-Induced Water Oxidation. *Chem. Mater.* **2015**, *27*, 5886–5891. [CrossRef]
16. Lan, J.; Wang, Y.; Huang, B.; Xiao, Z.; Wu, P. Application of polyoxometalates in photocatalytic degradation of organic pollutants. *Nanoscale Adv.* **2021**, *3*, 4646–4658. [CrossRef]
17. Streb, C.; Kastner, K.; Tucher, J. Polyoxometalates in photocatalysis. *Phys. Sci. Rev.* **2019**, *4*, 20170177. [CrossRef]
18. Wu, P.; Wang, Y.; Huang, B.; Xiao, Z. Anderson-type polyoxometalates: From structures to functions. *Nanoscale* **2021**, *13*, 7119–7133. [CrossRef]
19. Romo, S.; de Graaf, C.; Poblet, J.M. Mid-gap excitations in Anderson polyoxometalates. *Chem. Phys. Lett.* **2008**, *450*, 391–395. [CrossRef]
20. Wang, L.; Fu, W.; Zhuge, Y.; Wang, J.; Yao, F.; Zhong, W.; Ge, X. Synthesis of polyoxometalates (POM)/TiO_2/Cu and removal of nitrate nitrogen in water by photocatalysis. *Chemosphere* **2021**, *278*, 130298. [CrossRef]
21. Yu, J.; Wang, T.; Rtimi, S. Magnetically separable TiO_2/FeOx/POM accelerating the photocatalytic removal of the emerging endocrine disruptor: 2,4-dichlorophenol. *Appl. Catal. B Environ.* **2019**, *254*, 66–75. [CrossRef]
22. Jin, H.; Wu, Q.; Pang, W. Photocatalytic degradation of textile dye X-3B using polyoxometalate–TiO_2 hybrid materials. *J. Hazard. Mater.* **2007**, *141*, 123–127. [CrossRef] [PubMed]
23. Tang, Q.; An, X.; Lan, H.; Liu, H.; Qu, J. Polyoxometalates/TiO_2 photocatalysts with engineered facets for enhanced degradation of bisphenol A through persulfate activation. *Appl. Catal. B Environ.* **2020**, *268*, 118394. [CrossRef]
24. Su, T.; Chi, M.; Chang, H.; Jin, Y.; Liao, W.; Ren, W.; Zhao, D.; Len, C.; Lü, H. Enhanced oxidative desulfurization of fuel in ionic liquid by TiO_2 quantum dots catalysts modified with Anderson-type polyoxometalate. *Colloids Surf. A Physicochem. Eng. Asp.* **2022**, *632*, 127821. [CrossRef]
25. Sułek, A.; Pucelik, B.; Kuncewicz, J.; Dubin, G.; Dąbrowski, J.M. Sensitization of TiO_2 by halogenated porphyrin derivatives for visible light biomedical and environmental photocatalysis. *Catal. Today* **2019**, *335*, 538–549. [CrossRef]
26. Vallejo, W.; Diaz-Uribe, C.; Cantillo, Á. Methylene blue photocatalytic degradation under visible irradiation on TiO_2 thin films sensitized with Cu and Zn tetracarboxy-phthalocyanines. *J. Photochem. Photobiol. A Chem.* **2015**, *299*, 80–86. [CrossRef]
27. Ramamoorthy, R.; Radha, N.; Maheswari, G.; Anandan, S.; Manoharan, S.; Victor Williams, R. Betalain and anthocyanin dye-sensitized solar cells. *J. Appl. Electrochem.* **2016**, *46*, 929–941. [CrossRef]
28. Ludin, N.A.; Al-Alwani Mahmoud, A.M.; Bakar Mohamad, A.; Kadhum, A.A.H.; Sopian, K.; Abdul Karim, N.S. Review on the development of natural dye photosensitizer for dye-sensitized solar cells. *Renew. Sustain. Energy Rev.* **2014**, *31*, 386–396. [CrossRef]
29. Vallejo, W.; Rueda, A.; Díaz-Uribe, C.; Grande, C.; Quintana, P. Photocatalytic activity of graphene oxide–TiO_2 thin films sensitized by natural dyes extracted from Bactris guineensis. *R. Soc. Open Sci.* **2019**, *6*, 181824. [CrossRef]
30. Duan, M.Y.; Li, J.; Mele, G.; Wang, C.; Lü, X.F.; Vasapollo, G.; Zhang, F.X. Photocatalytic activity of novel tin porphyrin/TiO_2 based composites. *J. Phys. Chem. C* **2010**, *114*, 7857–7862. [CrossRef]
31. Min, K.S.; Kumar, R.S.; Lee, J.H.; Kim, K.S.; Lee, S.G.; Son, Y.A. Synthesis of new TiO_2/porphyrin-based composites and photocatalytic studies on methylene blue degradation. *Dyes Pigments* **2019**, *160*, 37–47. [CrossRef]
32. Su, X.Q.; Li, J.; Zhang, Z.Q.; Yu, M.M.; Yuan, L. Cu(II) porphyrins modified TiO_2 photocatalysts: Accumulated patterns of Cu(II) porphyrin molecules on the surface of TiO_2 and influence on photocatalytic activity. *J. Alloys Compd.* **2015**, *626*, 252–259. [CrossRef]
33. Zhang, W.; Wang, C.; Liu, X.; Li, J. Enhanced photocatalytic activity in porphyrin-sensitized TiO_2 nanorods. *J. Mater. Res.* **2017**, *32*, 2773–2780. [CrossRef]
34. Otieno, S.; Lanterna, A.E.; Mack, J.; Derese, S.; Amuhaya, E.K.; Nyokong, T.; Scaiano, J.C. Solar Driven Photocatalytic Activity of Porphyrin Sensitized TiO_2: Experimental and Computational Studies. *Molecules* **2021**, *26*, 3131. [CrossRef] [PubMed]
35. Zhu, Y.; Huang, Y.; Li, Q.; Zang, D.; Gu, J.; Tang, Y.; Wei, Y. Polyoxometalate-Based Photoactive Hybrid: Uncover the First Crystal Structure of Covalently Linked Hexavanadate-Porphyrin Molecule. *Inorg. Chem.* **2020**, *59*, 2575–2583. [CrossRef] [PubMed]
36. Liu, R.; Sun, Z.; Zhang, Y.; Xu, L.; Li, N. Polyoxometalate-modified TiO_2 nanotube arrays photoanode materials for enhanced dye-sensitized solar cells. *J. Phys. Chem. Solids* **2017**, *109*, 64–69. [CrossRef]
37. Ghali, M.; Brahmi, C.; Benltifa, M.; Vaulot, C.; Airoudj, A.; Fioux, P.; Dumur, F.; Simonnet-Jégat, C.; Morlet-Savary, F.; Jellali, S.; et al. Characterization of polyoxometalate/polymer photo-composites: A toolbox for the photodegradation of organic pollutants. *J. Polym. Sci.* **2021**, *59*, 153–169. [CrossRef]
38. Saad, A.; Rousseau, G.; El Moll, H.; Oms, O.; Mialane, P.; Marrot, J.; Parent, L.; Mbomekallé, I.M.; Dessapt, R.; Dolbecq, A. Molybdenum Bisphosphonates with Cr(III) or Mn(III) Ions. *J. Clust. Sci.* **2013**, *25*, 795–809. [CrossRef]
39. Giovannetti, R. The Use of Spectrophotometry UV-Vis for the Study of Porphyrins. In *Macro to Nano Spectroscopy*; Uddin, J., Ed.; InTech: London, UK, 2012; ISBN 987-953-51-0664-7.

40. Yan, W.; Hoekman, S.K.; Broch, A.; Coronella, C.J. Effect of hydrothermal carbonization reaction parameters on the properties of hydrochar and pellets. *Environ. Prog. Sustain. Energy* **2014**, *33*, 676–680. [CrossRef]
41. Yu, H.; Zhai, Y.; Dai, G.; Ru, S.; Han, S.; Wei, Y. Transition-Metal-Controlled Inorganic Ligand-Supported Non-Precious Metal Catalysts for the Aerobic Oxidation of Amines to Imines. *Chem.—Eur. J.* **2017**, *23*, 13883–13887. [CrossRef]
42. Lu, D.; Zhang, X.; Chen, H.; Lin, J.; Liu, Y.; Chang, B.; Qiu, F.; Han, S.; Zhang, F. A high performance solid-state asymmetric supercapacitor based on Anderson-type polyoxometalate-doped graphene aerogel. *Res. Chem. Intermed.* **2019**, *45*, 3237–3250. [CrossRef]
43. Küçük, İ.; Vural, S.; Kıvılcım, N.; Adıgüzel, İ.; Köytepe, S.; Seçkin, T. Preparation of the copper-based polyoxometalate/polyurethane composites and their dielectric properties. *Polym. Polym. Compos.* **2019**, *28*, 473–483. [CrossRef]
44. Grama, L.; Boda, F.; Gaz Florea, A.S.; Curticăpean, A.; Muntean, D.-L. The UV and IR Comparative Spectrophotometric Study of Some Saturated and Lacunary Polyoxometalates. *Acta Med. Marisiensis* **2014**, *60*, 84–88. [CrossRef]
45. Diaz-Uribe, C.E.; Rodríguez, A.; Utria, D.; Vallejo, W.; Puello, E.; Zarate, X.; Schott, E. Photocatalytic degradation of methylene blue by the Anderson-type polyoxomolybdates/TiO_2 thin films. *Polyhedron* **2018**, *149*, 163–170. [CrossRef]
46. Khoshnavazi, R.; Sohrabi, H.; Bahrami, L.; Amiri, M. Photocatalytic activity inhancement of TiO_2 nanoparticles with lanthanide ions and sandwich-type polyoxometalates. *J. Sol-Gel Sci. Technol.* **2017**, *83*, 332–341. [CrossRef]
47. Li, J.H.; Wang, X.L.; Song, G.; Lin, H.Y.; Wang, X.; Liu, G.C. Various Anderson-type polyoxometalate-based metal–organic complexes induced by diverse solvents: Assembly, structures and selective adsorption for organic dyes. *Dalt. Trans.* **2020**, *49*, 1265–1275. [CrossRef] [PubMed]
48. Miculescu, F.; Luță, C.; Constantinescu, A.E.; Maidaniuc, A.; Mocanu, A.C.; Miculescu, M.; Voicu, Ș.I.; Ciocan, L.T. Considerations and Influencing Parameters in EDS Microanalysis of Biogenic Hydroxyapatite. *J. Funct. Biomater.* **2020**, *11*, 82. [CrossRef] [PubMed]
49. Diaz-Uribe, C.E.; Daza, M.C.; Páez-Mozo, E.A.; Martínez, O.F.; Guedes, C.L.B.; Di Mauro, E. Visible light singlet oxygen production with tetra(4-carboxyphenyl)porphyrin/SiO_2. *J. Photochem. Photobiol. A Chem.* **2013**, *259*, 47–52. [CrossRef]
50. Huang, C.; Lv, Y.; Zhou, Q.; Kang, S.; Li, X.; Mu, J. Visible photocatalytic activity and photoelectrochemical behavior of TiO_2 nanoparticles modified with metal porphyrins containing hydroxyl group. *Ceram. Int.* **2014**, *40*, 7093–7098. [CrossRef]
51. Al-Ghouti, M.A.; Da'ana, D.A. Guidelines for the use and interpretation of adsorption isotherm models: A review. *J. Hazard. Mater.* **2020**, *393*, 122383. [CrossRef]
52. Li, M.; Zhao, H.; Lu, Z.Y. Porphyrin-based porous organic polymer, Py-POP, as a multifunctional platform for efficient selective adsorption and photocatalytic degradation of cationic dyes. *Microporous Mesoporous Mater.* **2020**, *292*, 109774. [CrossRef]
53. Wang, N.; Chen, J.; Wang, J.; Feng, J.; Yan, W. Removal of methylene blue by Polyaniline/TiO_2 hydrate: Adsorption kinetic, isotherm and mechanism studies. *Powder Technol.* **2019**, *347*, 93–102. [CrossRef]
54. Ayawei, N.; Ebelegi, A.N.; Wankasi, D. Modelling and Interpretation of Adsorption Isotherms. *J. Chem.* **2017**, *2017*, 3039817. [CrossRef]
55. Geng, Y.; Zhang, J.; Zhou, J.; Lei, J. Study on adsorption of methylene blue by a novel composite material of TiO_2 and alum sludge. *RSC Adv.* **2018**, *8*, 32799. [CrossRef] [PubMed]
56. Naseri, K.; Allahverdi, A. Methylene blue adsorption by TiO_2-based nano-adsorbents: Performance evaluation and kinetic study. *Res. Chem. Intermed.* **2019**, *45*, 4863–4883. [CrossRef]
57. Hou, Y.; Sun, J.; Zhang, D.; Qi, D.; Jiang, J. Porphyrin–Alkaline Earth MOFs with the Highest Adsorption Capacity for Methylene Blue. *Chem.—Eur. J.* **2016**, *22*, 6345–6352. [CrossRef]
58. Qin, L.; Pan, Y.; Xie, F.; Yu, L.; Huai, R.; Yang, L.; Zhang, D.; Zhou, Z. Rapid and selective adsorption capacity towards cationic dye with an anionic functionalized Anderson-type polyoxometalate. *Inorg. Chem. Commun.* **2021**, *133*, 108988. [CrossRef]
59. Saha, P.; Chowdhury, S.; Gupta, S.; Kumar, I. Insight into adsorption equilibrium, kinetics and thermodynamics of Malachite Green onto clayey soil of Indian origin. *Chem. Eng. J.* **2010**, *165*, 874–882. [CrossRef]
60. Konstantinou, I.K.; Albanis, T.A. TiO_2-assisted photocatalytic degradation of azo dyes in aqueous solution: Kinetic and mechanistic investigations: A review. *Appl. Catal. B Environ.* **2004**, *49*, 1–14. [CrossRef]
61. Sahoo, T.R.; Prelot, B. Adsorption Processes for the Removal of Contaminants from Wastewater: The Perspective Role of Nanomaterials and Nanotechnology. In *Nanomaterials for the Detection and Removal of Wastewater Pollutants*; Elsevier: Amsterdam, The Netherlands, 2020; pp. 161–222.
62. Scrimieri, L.; Velardi, L.; Serra, A.; Manno, D.; Ferrari, F.; Cantarella, M.; Calcagnile, L. Enhanced adsorption capacity of porous titanium dioxide nanoparticles synthetized in alkaline sol. *Appl. Phys. A Mater. Sci. Process.* **2020**, *126*, 926. [CrossRef]
63. Ibrahim, N.S.; Leaw, W.L.; Mohamad, D.; Alias, S.H.; Nur, H. A critical review of metal-doped TiO_2 and its structure–physical properties–photocatalytic activity relationship in hydrogen production. *Int. J. Hydrogen Energy* **2020**, *45*, 28553–28565. [CrossRef]
64. Nakata, K.; Fujishima, A. TiO_2 photocatalysis: Design and applications. *J. Photochem. Photobiol. C Photochem. Rev.* **2012**, *13*, 169–189. [CrossRef]
65. Wang, H.; Zhou, D.; Wu, Z.; Wan, J.; Zheng, X.; Yu, L.; Phillips, D.L. The visible light degradation activity and the photocatalytic mechanism of tetra(4-carboxyphenyl) porphyrin sensitized TiO_2. *Mater. Res. Bull.* **2014**, *57*, 311–319. [CrossRef]
66. Zhao, X.; Wang, Y.; Feng, W.; Lei, H.; Li, J. Preparation of Cu(II) porphyrin–TiO_2 composite in one-pot method and research on photocatalytic property. *RSC Adv.* **2017**, *7*, 52738–52746. [CrossRef]

67. Shalini, S.; Balasundaraprabhu, R.; Kumar, T.S.; Prabavathy, N.; Senthilarasu, S.; Prasanna, S. Status and outlook of sensitizers/dyes used in dye sensitized solar cells (DSSC): A review. *Int. J. Energy Res.* **2016**, *40*, 1303–1320. [CrossRef]
68. Ryu, J.; Kumar, R.S.; Son, Y.-A. Robust Photodegradation of Methylene Blue with the Biphenyl-Porphyrin/TiO_2 Photocatalyst Under Visible Light Condition. *J. Nanosci. Nanotechnol.* **2020**, *20*, 6266–6273. [CrossRef]
69. Lee, U.; Joo, H.-C.; Kwon, J.-S. Tetraammonium hexa hydrogen hexamolybdonickel ate(II) tetrahydrate, $(NH_4)_4[H_6NiMo_6O_{24}]\cdot 4H2O$. *Acta Crystallogr. Sect. E Struct. Rep. Online* **2002**, *58*, i6–i8. [CrossRef]
70. Adler, A.D.; Longo, F.R.; Shergalis, W. Mechanistic Investigations of Porphyrin Syntheses. I. Preliminary Studies on *ms*-Tetraphenylporphin. *J. Am. Chem. Soc.* **1964**, *86*, 3145–3149. [CrossRef]
71. Kontos, A.I.; Kontos, A.G.; Tsoukleris, D.S.; Bernard, M.-C.; Spyrellis, N.; Falaras, P. Nanostructured TiO_2 films for DSSCS prepared by combining doctor-blade and sol–gel techniques. *J. Mater. Process. Technol.* **2008**, *196*, 243–248. [CrossRef]
72. Quiñones, C.; Ayala, J.; Vallejo, W. Methylene blue photoelectrodegradation under UV irradiation on Au/Pd-modified TiO_2 films. *Appl. Surf. Sci.* **2010**, *257*, 367–371. [CrossRef]